Simulations on time-of-flight ERDA spectrometer performance

Jaakko Julin,[1, a)] Kai Arstila,[1] and Timo Sajavaara[1]
University of Jyväskylä, Department of Physics, P.O. Box 35, FI-40014 University of Jyväskylä, Finland

(Dated: 12 July 2016)

The performance of a time-of-flight spectrometer consisting of two timing detectors and an ionization chamber energy detector has been studied using Monte Carlo simulations for the recoil creation and ion transport in the sample and detectors. The ionization chamber pulses have been calculated using Shockley-Ramo theorem and the pulse processing of a digitizing data acquisition setup has been modeled. Complete time-of-flight–energy histograms were simulated under realistic experimental conditions. The simulations were used to study instrumentation related effects in coincidence timing and position sensitivity, such as background in time-of-flight – energy histograms. Corresponding measurements were made and simulated results are compared with data collected using the digitizing setup.

I. INTRODUCTION

In time-of-flight elastic recoil detection analysis (TOF-ERDA) atoms recoiling from samples are detected using timing detectors and an energy detector, typically either a silicon detector or a gas ionization chamber (GIC). The purpose of the energy detector is to enable mass separation of the recoils. Many of the spectrometers built in the past 15 years utilize heavy ion beams with energy around 10 MeV[1–4], and are used in the light element analysis of 10 nm to 300 nm thick films. Quite often the factors limiting the sensitivity are counting statistics and sample damage during the ion bombardment[5,6] rather than background, which has therefore remained largely unstudied. Time-of-flight ERDA has a low background, which is a result of the nature of coincidence measurements.

Gas ionization chambers are used in ToF-ERDA[2,7,8] due to their insensitivity to radiation damage and better resolution for heavy recoils compared to solid state detectors. The increasing use of GICs in this application has raised questions on their count rate and low energy performance, as well as position sensitivity.

Planar electrode gridded gas ionization chambers are inherently position sensitive in the direction perpendicular to the electrodes. The anode signal should be insensitive to position, giving a signal proportional to total electron charge while the cathode signal is proportional to both the total ionization and position. Position sensitivity can be achieved by comparing cathode and anode pulse heights, or by measuring the drift time of electrons to the Frisch grid[9,10]. Additionally splitting one of the electrodes into sawtooth segments can be used to achieve position sensitivity in the perpendicular direction.[10,11].

The Frisch grid shielding inefficiency and its influence to detector resolution has been studied previously[12]. The inefficiency is influenced by the aberrations of the electric field near the entrance window, making the contribution of the inefficiency to the anode signal recoil range dependent. These window effects also influence position resolution.

Using digitizers it is possible to capture different signals from a GIC and effects related to electron transport in the gas and the Frisch grid are open to study. See Fig. 1 for an example of cathode, grid and anode pulses captured from a GIC.

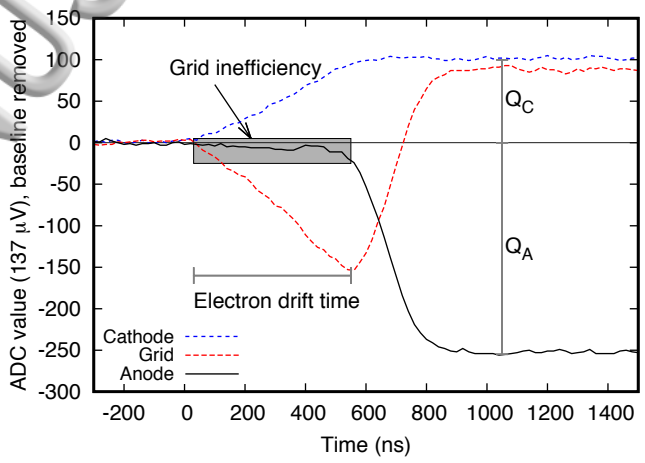

FIG. 1. Anode, Frisch grid and cathode pulses as digitized by a CAEN N6724 digitizer from a parallel plate GIC. The grid shielding inefficiency, electron drift time to anode and collected charges can be extracted from these pulses.

A Monte Carlo (MC) simulation code MCERD[13] has been developed to reproduce experimental ERDA energy spectra. Effects including the beam spot size, multiple and plural scattering and scattering in the detector foils are taken into account. The use of this MC method for analysis has been validated[14].

Here the MC simulation is further expanded to be useful in the study of a time-of-flight – energy telescope. The simulation codes developed in this study are aimed at studying the effects of the system as a whole, with the intent of simulating entire time-of-flight – energy histograms rather than some ions with fixed energy and recoiling angle from the target. The simulations enable the study of background due to count rate related issues such as false coincidences and pile-up in addition to effects related to energy detector response, e.g. position dependence and large angle scattering inside the gas ionization chamber.

[a)] Electronic mail: jaakko.julin@jyu.fi

This manuscript was accepted by Rev. Sci.Instrum. Click here to see the version of record.

Systematic studies related to detection limits of trace elements are difficult via direct measurements, since samples are damaged by ion bombardment and underlying effects may not be straightforward to quantify. Some of the background events are indistinguishable from proper events and therefore to get an estimate on their contribution simulations are necessary. Certain wrong coincidences can be detected and simulations can be used to reproduce these, providing additional evidence on the underlying background generating mechanisms.

II. SIMULATION SOFTWARE

A. MCERD

The existing ion transport and detector description in the code makes it possible to simulate either ideal energy detectors or time-of-flight detectors. For the purposes of this study it was enough to describe the time-of-flight detector as foils followed by the entrance window and the gas volume of the ionization chamber. As the ions enter the ionization chamber their energy, energy lost to collisions, position and time are tabulated. These data are used in the following stage to simulate the energy detector response.

One major modification to MCERD was the inclusion of recoil cascades, as previously the simulation tracked only one recoiled atom from the sample at a time. In the modified code sufficiently energetic recoils create more secondary recoils in the energy detector gas volume or in the entrance window. These secondary recoils are tracked and their movement is tabulated the same way as for the original recoil from the sample.

Additionally the program was made to output events that do not hit the ionization chamber, but pass through the first timing detector (T1) or the second timing detector (T2). This is possible if the solid angles of the detectors are different or due to large angle scattering in the carbon foils of the timing detectors. The SRIM 2013 code[15] was used as a source of electronic stopping data for various ions.

The geometry of simulated detectors and the beam spot are made to match the ToF-ERDA setup in Jyväskylä[4]. The flight distance is 623 mm and the detector angle is 41.3°. The beam spot size in the simulations was 2 mm by 3 mm, which creates a 6 mm by 3 mm beam spot projected on to the sample when the angle between the beam and sample normal is approximately 20°. See Fig. 3 for the geometry used in the simulations.

B. GIC response

The gas ionization chamber response is modeled using Shockley-Ramo theorem, which is commonly used to model a variety of radiation detectors which are based on moving charges[16]. The GIC simulation is intended to be simple and fast enough to simulate a large number of pulses in order to simulate entire measurements with hundreds of thousands of events each generating thousands or tens of thousands of electrons in the gas. The specific detector modeled here is described in Ref.[7].

The electric field and effective weighting potentials have been calculated in 2D using finite element method program FEMM 4.2[17]. The field between the electrodes was calculated in the xy plane perpendicular to the electrodes in xz plane. The electric potential $V(x, y)$ of the chamber is shown in Fig. 2. The calculated potentials and fields are sampled at 0.1 mm intervals in x and y directions, except near the Frisch grid, where the interval is 5 µm. The simulations use the tabulated data with bilinear interpolation.

Electrons are created along the path of the tracks of the ions, given by the MCERD calculated tracks. The production of electrons in the gas is based on the average energy loss per ion-pair produced, i.e. W values. There is no adequate theory or sufficient experimental data to approximate W, which has been shown to be mass, nuclear charge and energy dependent for heavy ions[18–20]. The differences are explained by energy and ion dependence on the ratio of cross sections for ionization and excitation and transfer of kinetic energy into kinetic energy of gas molecules[18].

For the purposes of this simulation the response of several ions in isobutane was measured using beams scattered from a gold target. Time-of-flight measurement was used to determine the energy before the ionization chamber. The energy lost in the carbon foils and the entrance window was subtracted using SRIM 2013 stopping values. The average energy required to produce an ion pair was calculated from these measurements over a broad energy range. The results for ^{1}H, ^{4}He, ^{12}C, ^{16}O, ^{28}Si and ^{63}Cu are plotted in Fig. 4. The measurements were also performed for ^{6,7}Li, ^{10,11}B, ^{27}Al, ^{29,30}Si, ^{35,37}Cl, ^{65}Cu, ^{79,81}Br, ^{127}I and ^{197}Au. Differences between isotopes were within experimental error at similar velocities.

The preamplifier and pulse processing chain were calibrated by injecting a known charge $Q = CV$ into the input of the preamplifier with the help of a pulser and a 0.5 pF capacitor. The pulses were then processed using a digitizer. Using the obtained calibration factor it is possible to calculate how much charge is collected by the anode. The goal was to obtain a relative calibration for all ions, therefore the uncertainties associated with the test capacitor and pulser calibration are not considered. There are uncertainties associated with the treatment of stopping in the entrance window, time-of-flight to energy calibration, fitting and smoothing of the data.

The response of isotopes or elements which are not measured can be estimated by interpolating the measured responses. The calibrations were extrapolated down to zero deposited energy. When the ion track is converted into an ionization track the same W is assumed for not only the incident particle but also the subsequent recoils in cascades. This way the W will be the same in simulations and measurements, but fluctuations in the total ionization due to the recoils is not accounted for.

The number of electrons can be subjected to a fluctuation to account for Fano noise. The Fano factor[21], like W is not strictly constant for different heavy ions and different energies, but these data are not available in the literature and have not been measured by the authors

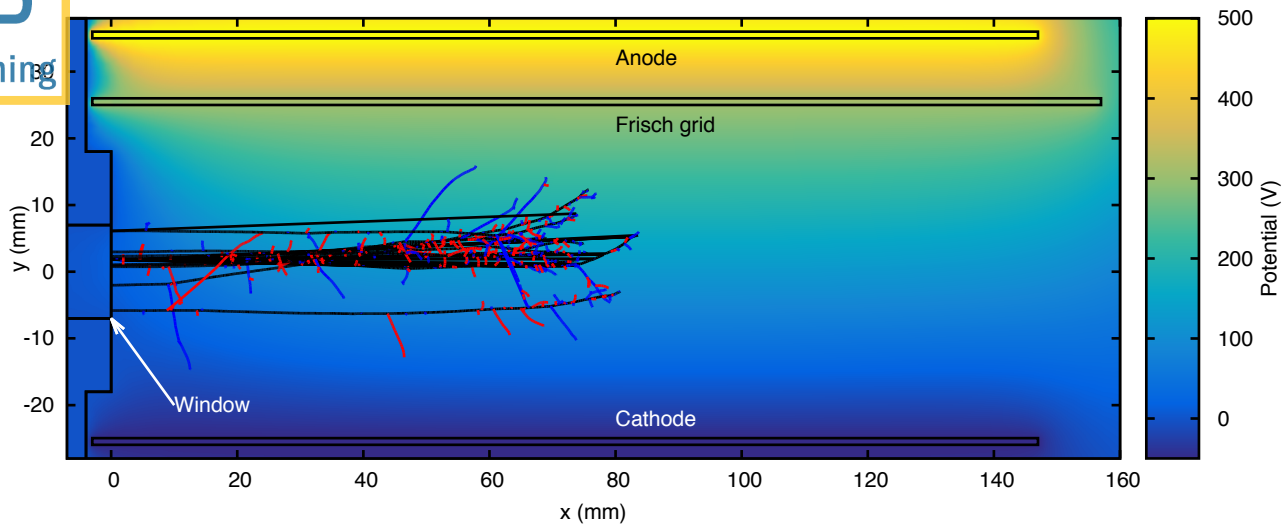

FIG. 2. Electric potential in the gas ionization chamber. The cathode, grid and anode voltages are −50 V, 300 V and 500 V, respectively. The primary recoils from the sample, 5 MeV to 7 MeV titanium, are plotted in black. Tracks of recoiling hydrogen and carbon atoms of the detector gas are plotted in red and blue, respectively. The entrance window is located at $x = 0$ mm.

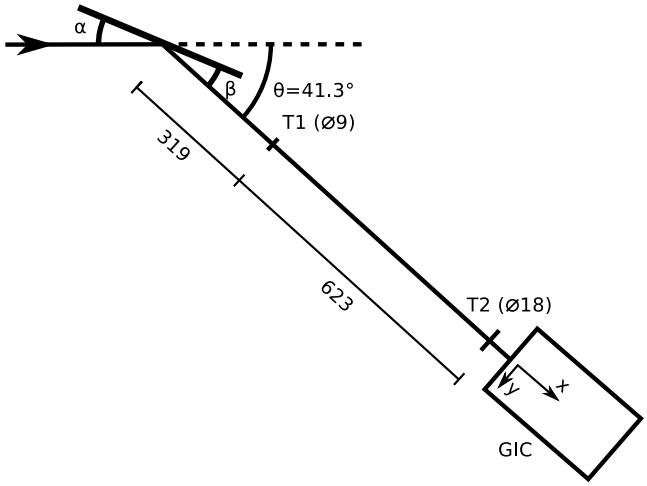

FIG. 3. The time-of-flight – energy spectrometer geometry used in the simulations. The xy-coordinates used in the gas ionization chamber simulations are marked inside the GIC. Mirror geometry ($\alpha = \beta \approx 20°$) was used. All dimensions are in mm. The diameter given for T1 and T2 correspond to the last aperture of the detectors, the GIC entrance window is a 14 mm × 14 mm square.

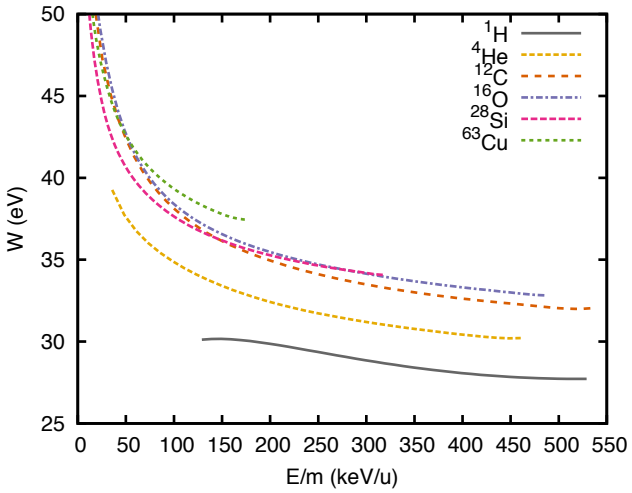

FIG. 4. Average energy required to produce an electron-ion pair for various ions in isobutane calculated from collected anode charge and energy determined from time-of-flight measurement is plotted. The results are presented for hydrogen, helium, carbon, oxygen, silicon and copper ions. The results may be significantly affected by systematic uncertainties described in the text.

either.

Slow tail caused by drifting ionized gas molecules is ignored, as the pulse of interest is determined primarily by the much faster moving electrons and the ion tail would be filtered out by pulse shaping. The anode is additionally shielded by the Frisch grid from the ion signal.

Electron transport in the gas is assumed to be collisional drifting motion along the electric field lines,

$$\frac{d\vec{x}}{dt} = -v_d(|E|)\hat{E}, \tag{1}$$

where E is the electric field, and v_d is the drift velocity.

The drift velocity is given by Ref.[22]. A simple diffusion model was implemented, where both transverse and longitudinal dispersion are given by

$$\sigma_x = \sqrt{\frac{2\epsilon_k}{eE}x}, \tag{2}$$

where x is the drift distance, ϵ_k is the characteristic energy at certain electric field and e is the elementary charge. The values used here were also given by Ref.[22]. The dispersion in each time step was close to numerical error. The simulations in this article were run without the dispersion model, since the contribution was negligible compared to variations in the initial distribution of

electrons.

It should be noted that the electron transport used here does not account for any effects near the scale given by the mean free path of the electrons. This approximation holds elsewhere in the studied system except near the Frisch grid. The code does not allow electrons to be captured by the wires of the Frisch grid. For more accurate models the reader is referred to more advanced simulations, such as Garfield[23], which can take into account many contributions ignored here, such as delta electrons, ion tail and full 3D effects.

Without the dispersion and initial kinetic energy each electron is transported deterministically and the induced charge on any electrode can be determined from the (x, y) coordinates directly. The characteristic pulse $f(x, y, t)$ was precalculated for each (x, y, t) point with 0.5 mm and 2 ns spacing. The pulse can now be calculated rapidly as a sum over n electrons

$$V(t) = \sum_{i=0}^{n} f(x_i, y_i, t - t_i), \tag{3}$$

where (x_i, y_i, t_i) is the position where the electron was born.

C. Telescope simulation

This simulation models the detectors, data acquisition and pulse processing of a digitizing setup[24]. The MCP signals from T1 and T2 timing detectors are digitized after amplification by a CAEN N6751 digitizer. The GIC anode and cathode signals are amplified with Amptek CoolFET preamplifiers and digitized using a CAEN N6724 digitizer. The pulse processing of the GIC signals is handled by the CAEN DPP-PHA processing on the FPGA, while time-of-flight signals are processed using software running on the computer reading out the digitizers.

1. Event generation

The events created by MCERD have a weight assigned to them, which is calculated from the distribution of the element in the sample and the cross section of the reaction. The telescope simulation builds a list of random events, in which the probability of event occurring is proportional to its weight. One MCERD-generated event can therefore appear in the output once or more or not at all. Calculating more events using MCERD will reduce the weight of an individual event in the telescope simulation. The time between events obeys Poisson statistics. The simulated count rate can be easily varied and so called dark counts, i.e. events not originating from a recoil, can be injected in to the stream of events with some predetermined count rate.

Individual events in the telescope simulation correspond to hits in the detectors. A list of hits in all detectors with picosecond time resolution is created. Energy detector hits have a unique identifier, which is used to couple the calculated electron pulse to the list of hits.

2. GIC pulse shaping

The ionization chamber pulses are simulated as described in section II B.

Up to five ideal overlapping electron charge pulses are summed and converted into waveforms resembling digitized data by applying the gain of the preamplifier (0.64 µV/electron) and the digitizer gain (137 µV/LSB). The samples of the waveform have a 20 ns interval, which corresponds to the waveforms acquired from the N6724 digitizer when it is used in a mode where two consecutive samples captured at 100 MS /s sampling rate are averaged. Noise is added to the waveform to simulate the electronics noise, which was assumed to be white, although the actual measured noise spectrum is somewhat different. In particular the real detector suffers from low frequency noise associated with vibrations and some intermittent higher frequency noise from external interference. The electronics noise of the studied system was measured with a pulser and white noise was added to simulated data so that after similar shaping the peak width is identical.

The preamplifier output rise time with typical detector capacitance 1 pF to 100 pF is less than 20 ns, which is short compared to the 300 ns to 500 ns current pulse from the ionization chamber and is also comparable to the 10 ns sampling interval used in the digitizing setup. The fall time RC constant is 500 µs, which is long enough to make any ballistic deficit minuscule. Preamplifier response is assumed to be ideal for these reasons.

The telescope simulation reproduces the operation of the trigger filter and pulse height filter of the CAEN digitizer. The trapezoidal pulse height filter used in the simulations is described by a recursive formula[25]

$$s(n) = s(n-1)+v(n)-v(n-k)-v(n-l)+v(n-l-k), \tag{4}$$

where $v(n)$ is the nth input sample and k is the rise time of the trapezoid and $l = k + m$, where m is the flat top duration of the filter. The time constants are expressed as a number of samples. The filter is similar to the trapezoidal filter used in the CAEN DPP-PHA firmware. In addition to the trapezoidal filter a RC-CR^2-like trigger filter used by the firmware has been modeled. The trigger filter has a window average, here 32 samples or 640 ns and a double derivation using a delay, here 1 µs, long enough to account for the rise time of the input signal and the slower rise due to averaging. The signals from a GIC are noticeably slower than those of a silicon detector and have worse signal to noise ratio, making the averaging a necessity. With these parameters the trigger filter can capture the full pulse amplitude from real detector signals and trigger even 100 keV pulses.

If two consecutive pulses can be separated by the trigger filter but not by the trapezoidal filter either the latter pulse or both pulses can be rejected by the pile-up inspector. A properly adjusted trapezoidal filter is therefore immune to pile-up except for pulses within the trigger filter delay parameter (1 µs). There is also a rise time discriminator implemented on the CAEN firmware, which rejects triggers with too long time between the threshold and zero crossing. However noisy signals and varying

rise times may prevent the efficient operation of the discriminator. Pile-up which affects the timing may also be rejected in a coincidence measurement by the coincidence criteria. In the simulations and measurements shown in this article the rise time discriminator was turned off.

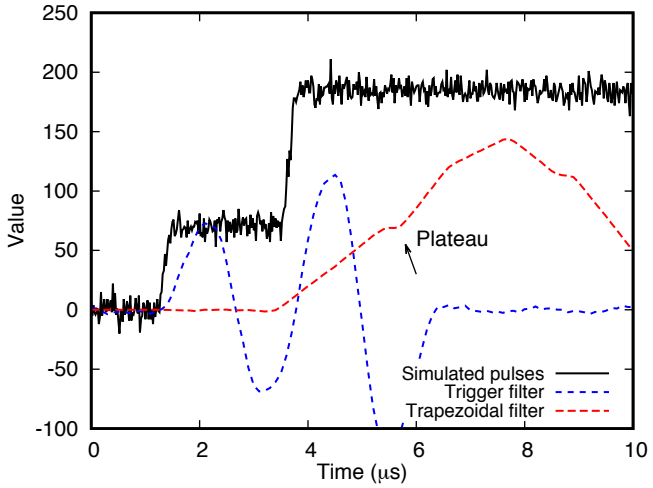

FIG. 5. Simulated pulses processed with the trigger filter and the trapezoidal filter with a rise time of 2 µs. Since the trapezoidal pulse height filter starts to plateau, the pulse height of the first event could have been determined correctly by the pulse height filter if the second event arrived any later. These pulses are however separated by the trigger filter and can be rejected by the pile-up inspector. This behavior is similar in simulations and in CAEN digitizer pulse height processing.

3. Timestamped list-mode data

The list of hits is sorted and the time-of-flight is determined by looking for the first T1 hit within the timing window before a T2 hit, as this is the same way the experimental apparatus determines the time-of-flight. Time-of-flight resolution was matched between simulations and measurements by applying gaussian noise to the list data. The output of this simulation is list-mode data, where timestamps are also subjected to similar jitter as the FPGA processing does with the digitizers.

4. List-mode coincidence

The timestamped list-mode data is processed with the same tools that are used in actual measurements. The coincidences between energy and time-of-flight are found by triggering a search from every energy event and accepting the first time-of-flight event within a specified time window.

III. EXPERIMENTAL

The experimental apparatus is described in references[4,7,24]. The spectrometer is installed to a 41.3° angle relative to the beam and has a time-of-flight distance of 623 mm. The timing resolution is approximately 180 ps. The measured spectra were obtained using a 13.3 MeV $^{63}Cu^{7+}$ beam and mirror geometry. The sample was an 80 nm thick atomic layer deposited TiO2 film on silicon substrate with some hydrogen and chlorine impurities in the film.

A. Verification of simulations

The simulations should match the observed behavior of the experimental apparatus so general observations can be made. As a reference the TiO2 sample was measured with an energy detector count rate of 1100 cps. The first 350000 coincidence counts are shown in 2D histogram in Fig. 6.

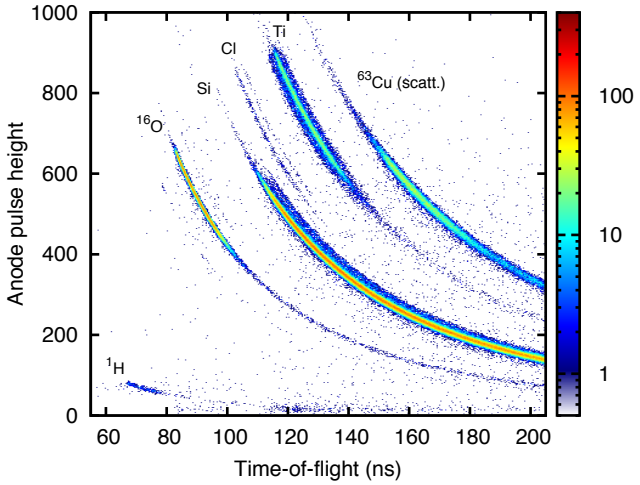

FIG. 6. Measured ToF–E histogram of the 80 nm thick TiO2 sample with a 13.3 MeV $^{63}Cu^{7+}$ beam.

In the measurements the anode pulse shape suggested a much greater grid shielding inefficiency than predicted by the simulations. This effect has also been observed by others[12] and is attributed to capacitive coupling between the grid and the anode. By replacing the preamplifier connected to the grid electrode with a lower impedance path to ground the coupling was greatly reduced, see Fig. 7. The simulations still seem to underestimate the shielding inefficiency, but this is most likely due to assumption of a flawless Frisch grid. The nonuniform spacing of the wires and wire sag could increase the inefficiency.

The rounding near the full amplitude of the anode pulse in Fig. 7 can be attributed to a long collection time of electrons originating near the window. The drift velocity is lower and the drift path to anode is longer for these electrons than those produced deeper inside the detector, since the electric field near the window is low and not perpendicular to the electrodes.

The electric field near the window could differ from simulations, due to uncertainty in electrode alignment and charging of the silicon nitride window. The rise time of simulated pulses is generally somewhat shorter.

The time-of-flight–energy event timestamp difference is plotted as a function of the time-of-flight in Fig. 8. The

recoils will need some ns to tens of ns to travel from T2 to the GIC and be stopped. The electrons created in the gas drift for a few hundred ns. The timestamp difference between T2 and GIC therefore varies primarily based on the drift time.

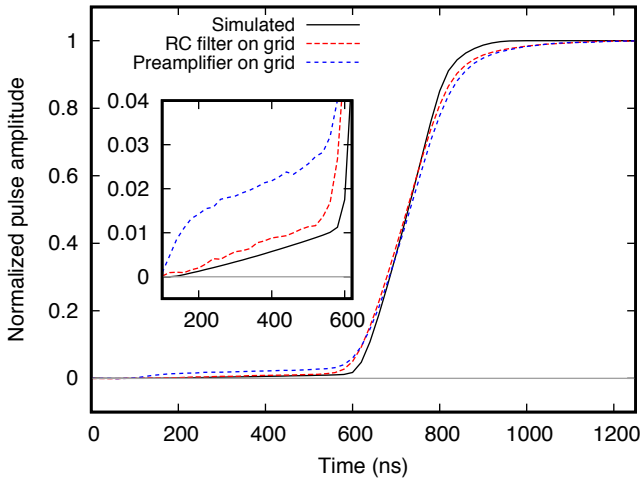

FIG. 7. Frisch grid shielding inefficiency and the influence of grid coupling. The simulated detector underestimates both the grid shielding inefficiency (inset) and the slow saturation of the collected charge. Measured and simulated pulses of oxygen recoils were normalized and averaged. The recoils were selected so that they have similar timestamp difference, i.e. same position in recoil plane.

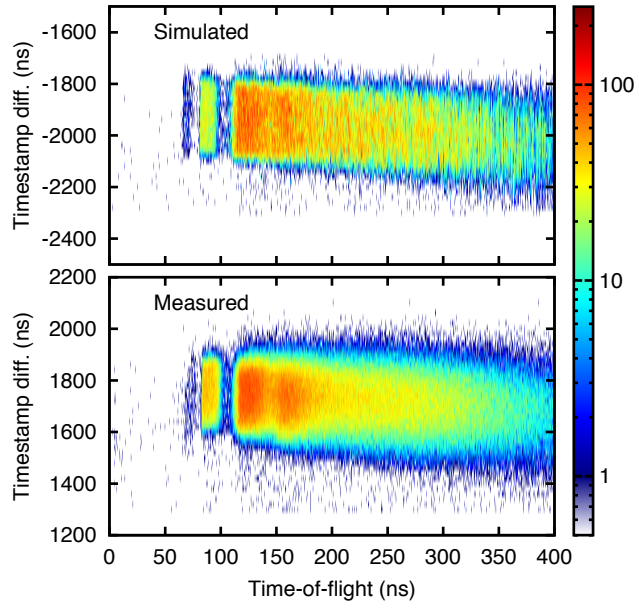

FIG. 8. Simulated and measured anode - T2 timestamp difference as a function of the time-of-flight. The width (vertical axis) of these curves is the difference in drift time between recoils entering the detector near either side of the entrance window.

IV. RESULTS

A. GIC position sensitivity

The Frisch grid shielding inefficiency is one source of pulse height deficit, i.e. the improper shielding will result in position dependent reduction in observed anode pulse height, see Fig. 9. The residual anode pulse position sensitivity is affected by signal shaping. With the flat top duration of the trapezoid set longer than the drift time ($> 1\,\mu s$) the inefficiency is integrated completely. Lower flat top and rise time values will reduce the effect.

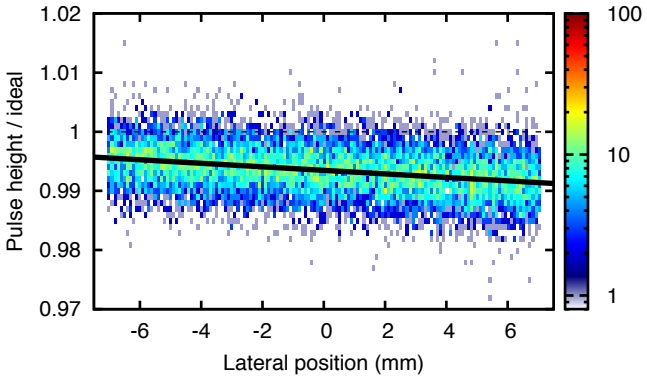

FIG. 9. Normalized anode pulse height vs lateral position, i.e. position at the detector window in the scattering plane (y), for approximately 4 MeV simulated oxygen recoils. There is a minor position dependent pulse height deficit associated with grid inefficiency.

The measurement of position via drift time analysis was also studied using the simulations. Experimentally it was found[7] that the drift time as determined by timestamp differences was accurate enough for kinematic correction. The simulations show that the drift time is quite well linear for typical recoils from the sample and the position resolution is better than cathode – anode pulse height comparison. The reason for the linearity in the presence of window aberrations is due to the trigger filter of the digitizer, which uses a 50% constant fraction for timing. The window aberrations influence only the latter part of the pulse, making the 50% value virtually immune to window effects.

In Fig. 10 the simulated timestamp difference of oxygen recoils has been plotted as a function of the lateral position at the GIC window. The position resolution is better than 2 mm given a timing resolution of 30 ns. Uncertainties in calibration can increase this further.

B. Mechanisms of background

Background is defined in this article to be any event where the energy (ionization signal) does not match the time-of-flight. Any event outside the 2D "bananas" is therefore clearly background, but this does not directly contribute to the results of any ERD analysis, since only the events inside the bananas are of relevance. However

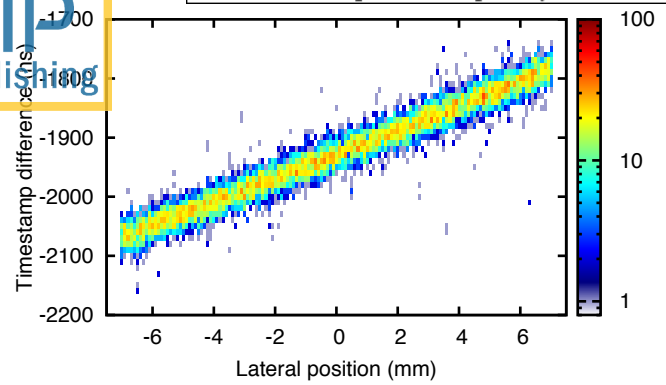

FIG. 10. Simulated anode - T2 timestamp difference as a function of lateral position of oxygen recoils at the entrance to the GIC (y). The drift time of electrons to the anode can be used to measure the recoil position.

there can be background events also in these regions of interest, which becomes evident when trace concentrations are studied.

Different mechanisms producing background have been studied, some of these effects are related to the spectrometer as a whole, and others are single detector effects.

1. Wrong time-of-flight–energy coincidence

Wrong time-of-flight–energy coincidence background happens when two particles arrive consecutively in T1 and in T2 and the first particle does not hit the energy detector. In this type of background there is practically no correlation between energy and time-of-flight. Wide coincidence window makes this type of background important at high count rates. This is further exacerbated if there is a difference in solid angles between time-of-flight detectors and the energy detector.

Rejecting this type of background relies on the ability to resolve T1 and T2 hits within the time-of-flight window, which is possible with some TDCs and digitizers assuming minimal ringing in MCP signals. In the system simulated here such rejection was not used.

2. Wrong T1 - T2 coincidence

Wrong T1 and T2 coincidence happens when a recoil is overtaken by another after T1, but before T2. This results in the time-of-flight being shorter than what it was supposed to be for the first particle and longer than expected for the second. The energy signal might lead to pileup, unless one of the recoils doesn't hit the energy detector. This source of background is therefore quite similar to the previously discussed one.

Some low energy background is also created by recoils which have a time-of-flight longer than the timing window. In an inverted start system like the one here, a T1 hit might not be detected. If a T1 hit is provided by another particle, some random time-of-flight background is generated.

3. Pile-up

Two consecutive recoils can create a signal in the ionization chamber, which is falsely interpreted as a single hit.

In a 2D time-of-flight–energy histogram the pile-up background mostly affects the region of heavy masses, especially if there are a lot of events from the substrate, such as silicon, or from scattered beam. Some of this background overlaps with wrong coincidence background as it is probable that events pile-up with events from substrate.

4. Scattering in GIC window or gas

Some background events are observed at low energies, but with apparently correct time-of-flight. The simulations show a similar behaviour. The energy loss in the simulations occurs when an atom of the entrance window is recoiled with some significant energy transfer. The energy lost by the first particle and one or more subsequent recoils in the window reduces the pulse height. Similar mechanism is possible in silicon detectors where the dead layer acts similarly to the window of the GIC.

Scattering in the detector gas contributes to background in $\Delta E - E$ detectors, as then the recoil causes an increase in signal at the ΔE portion[5,26]. For detectors with a single anode this effect is not observed. Large angle scattering in the gas can be reflected in the pulse shapes, but a major change in the pulse height requires either the recoil from the sample or the recoiled gas atom to hit an electrode or be ejected from the active volume. None of the measured digitized pulses could be unambiguously identified having a differing shape due to scattering in the gas.

When the pressure in the real GIC was reduced to below 10 mbar a dramatic degradation in mass resolution was observed, see Fig 11(c). The reproduction of this in simulations requires accurate stopping and straggling data. In Fig. 11(d) pressure of 10 mbar was simulated. The degradation of resolution is observed for recoils with the longest range. Even in this somewhat extreme case the degradation is mainly due to ions having a range longer than the anode length, not due to recoiling gas atoms.

The recoiling hydrogen atoms of the detector gas with a long enough range to hit the electrodes carry only a small amount of the total energy. The choice to use a constant W in spite of recoil cascades will slightly underestimate the recoiling hydrogen gas atom effect in the simulations.

5. Halos

The halo around light masses, most notably hydrogen, has been explained by MCP related effects[4]. The halo extends by only a few nanoseconds to either longer or shorter times-of-flight and is uncorrelated with the energy measurement, therefore the halos rarely overlap with

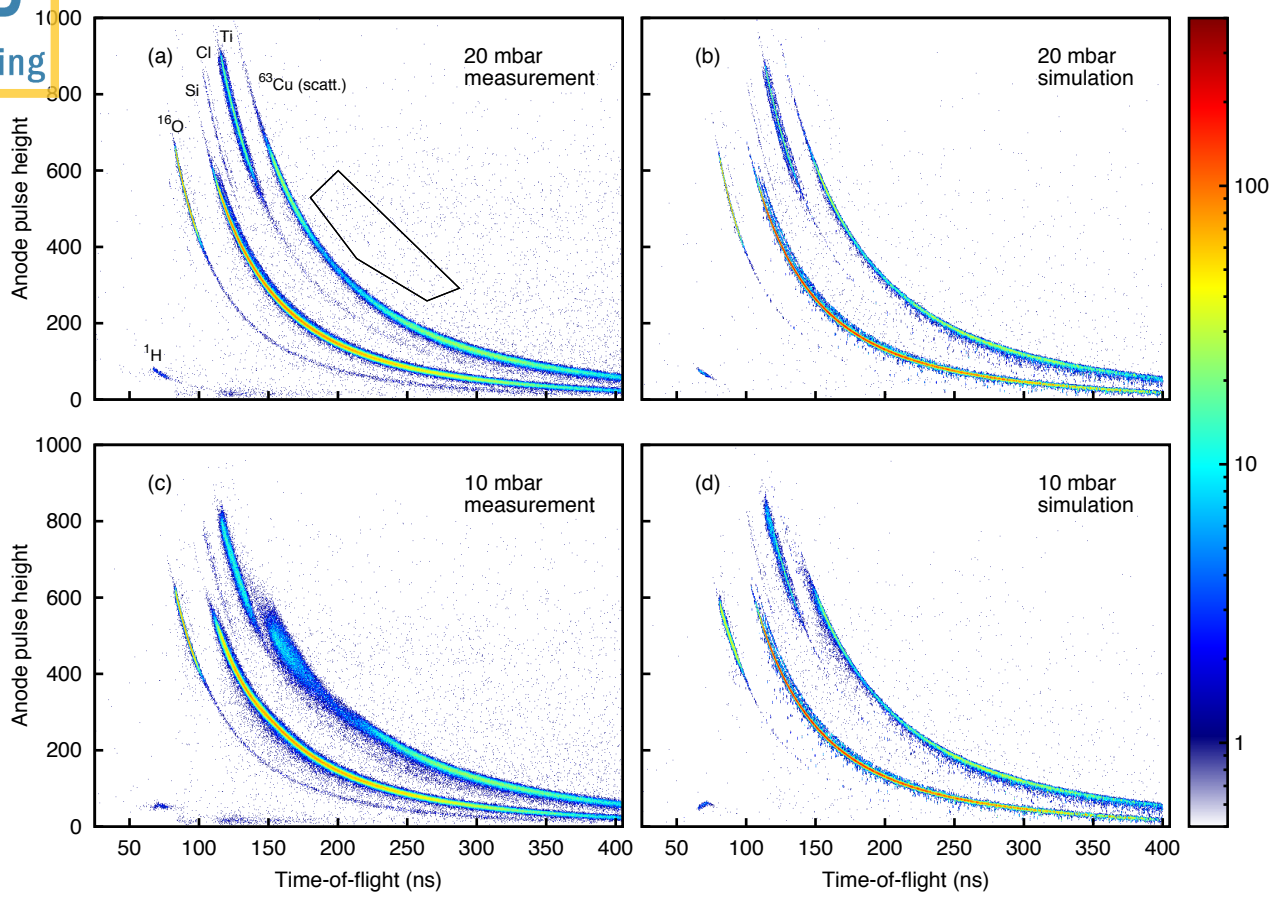

FIG. 11. Time-of-flight–E histograms of the TiO2 sample. The histogram (a) was measured and (b) was simulated with 20 mbar GIC pressure, which is sufficient to stop all recoils in the active volume. The histogram (c) was measured and (d) was simulated with 10 mbar pressure. Each of the histograms have 350000 events in total. The area inside the polygon in (a) corresponds to the 'Heavy' region in Fig. 12.

neighboring masses.

C. Background intensity

Assuming different count rates the relative intensities of different sources of background can be quantified in different regions of interest. In Fig. 11(b) a 2D ToF–E histogram is plotted with 10 000 cps T1 count rate. The number of events in different 2D regions, as the count rate was varied, is plotted in Fig. 12. The ^{1}H and ^{35}Cl regions are defined by a tight polygon around the masses of interest. The region labeled as 'Heavy' covers an ideally empty part of the 2D histogram, where recoils heavier than Cu would be expected. The region is marked in Fig. 11. A linear increase of counts in the area of heavy masses can be observed. Both the wrong coincidences and pile-up are expected to increase linearly with increasing count rate. The chlorine 'Cl' region covers both ^{35}Cl and ^{37}Cl, even though they can be separated in practice. If unnecessarily large polygon selections are made like in this case or elements with multiple unseparable isotopes are analyzed it can be seen that the number of events inside the region at high count rates is exaggerated.

The increase of long time-of-flight wrong coincidences causes some short time-of-flight events to be rejected, which in turn reduces the number of observed counts in the hydrogen region, even though there is a small but increasing number of background events also in the same region.

The measured histogram Fig. 11(a) shows much more background compared to the simulated one, Fig. 11(b). The difference is suspected to be partially due to low energy sputtered atoms, which cause a notable increase in T1 count rate in measurements.

V. CONCLUSIONS

A gas ionization chamber as the energy detector in a time-of-flight ERDA has unarguably improved the mass resolution of the spectrometer, justifying most of the limitations it possibly has.

These simulations provide valuable details on problems and limitations in the design and means to study them before detectors are built. The simulations provide further incentive to have as thin entrance window as possible, not merely because of the electronic energy loss and straggling in it, but also due to energy transfer to recoils within the window. Rise time of the anode pulses

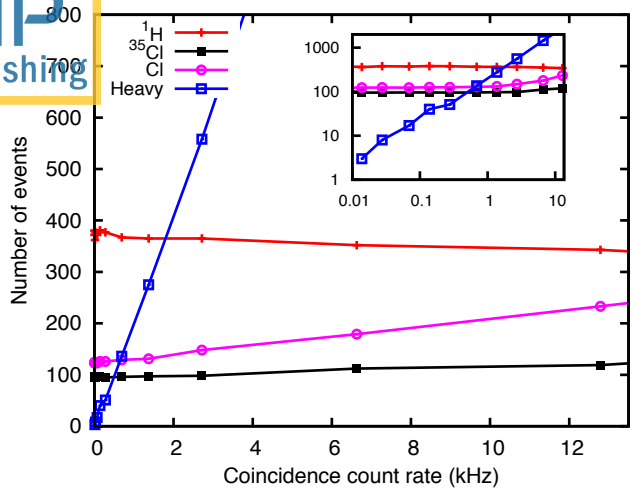

FIG. 12. Total number of events inside 2D regions with different count rates in the simulation. The regions are explained in the text. The same events were created with the same relative time differences between events. The variation in number of events is therefore purely due to count rate dependent mechanisms. The inset shows the same data on a different scale.

could be improved by increasing the electric field in the near-window region, and can be achieved by biasing the window. This would likely improve the position resolution and shorter rise time would also reduce pile-up and wrong coincidences.

The simulations provided means to verify the position sensitivity of an existing GIC design, and supported the results of previous experimental studies. The various mechanisms with which background is generated in time-of-flight–energy spectra were studied. Care should be taken with both data acquisition and ionization chamber design if count rates exceeding 1 kHz are to be used in low background measurements.

The gas ionization simulations could be improved by solving the electrostatic problems in three dimensions and implementing models which take into account the random motion of electrons in the gas. The fundamental knowledge of average ionization yields and variation in those for heavy ions of different energies in the detector gases would improve the predictability of mass resolution of time-of-flight–energy spectrometers.

ACKNOWLEDGMENTS

This work was supported by the Finnish Funding Agency for Technology and Innovation Tekes through EU regional funds project HIUDAKE and Academy of Finland Center of Excellence in Nuclear and Accelerator Based Physics (Ref. 251353).

[1] A. Razpet, P. Pelicon, Z. Rupnik, and M. Budnar, Nucl. Instrum. Meth. B **201**, 535 (2003).
[2] C. Kottler, M. Döbeli, F. Glaus, and M. Suter, Nucl. Instrum. Meth. B **248**, 155 (2006).
[3] S. Giangrandi, T. Sajavaara, B. Brijs, K. Arstila, A. Vantomme, and W. Vandervorst, Nucl. Instrum. Meth. B **266**, 5144 (2008).
[4] M. Laitinen, M. Rossi, J. Julin, and T. Sajavaara, Nucl. Instrum. Meth. B **337**, 55 (2014).
[5] G. Dollinger, M. Boulouednine, A. Bergmaier, T. Faestermann, and C. M. Frey, Nucl. Instrum. Meth. B **118**, 291 (1996).
[6] S. R. Walker, J. A. Davies, J. S. Forster, S. G. Wallace, and A. C. Kockelkoren, Nucl. Instrum. Meth. B **136-138**, 707 (1998).
[7] J. Julin, M. Laitinen, and T. Sajavaara, Nucl. Instrum. Meth. B **332**, 271 (2014).
[8] Z. Siketić, N. Skukan, and I. Bogdanović Radović, Rev. Sci. Instrum. **86**, 083301 (2015).
[9] W. Assmann, Nucl. Instrum. Meth. B **64**, 267 (1992).
[10] A. Bergmaier, G. Dollinger, and C. M. Frey, Nucl. Instrum. Meth. B **136-138**, 638 (1998).
[11] H. Timmers, T. R. Ophel, and R. G. Elliman, Nucl. Instrum. Meth. B **156**, 236 (1999).
[12] A. Göök, F.-J. Hambsch, A. Oberstedt, and S. Oberstedt, Nucl. Instrum. Meth. A **664**, 289 (2012).
[13] K. Arstila, T. Sajavaara, and J. Keinonen, Nucl. Instrum. Meth. B **174**, 163 (2001).
[14] N. Barradas, K. Arstila, G. Battistig, M. Bianconi, N. Dytlewski, C. Jeynes, E. Kótai, G. Lulli, M. Mayer, E. Rauhala, E. Szilágyi, and M. Thompson, Nucl. Instrum. Meth. B **262**, 281 (2007).
[15] J. F. Ziegler, M. D. Ziegler, and J. Biersack, Nucl. Instrum. Meth. B **268**, 1818 (2010).
[16] Z. He, Nucl. Instrum. Meth. A **463**, 250 (2001).
[17] D. C. Meeker, "Finite Element Method Magnetics," `http://www.femm.info/`.
[18] ICRU Report 31, *Average Energy Required to Produce An Ion Pair* (ICRU, Washington, D.C. USA, 1979).
[19] J. M. Valentine and S. C. Curran, Rep. Prog. Phys. **21**, 1 (1958).
[20] M. Chemtob, B. Lavigne, J. Chary, V. D. Nguyen, N. Parmentier, J. P. Noel, and C. Fiche, Phys. Med. Biol. **22**, 208 (1977).
[21] U. Fano, Phys. Rev. **70**, 44 (1946).
[22] G. Schultz and J. Gresser, Nucl. Instrum. Methods **151**, 413 (1978).
[23] R. Veenhof, Nucl. Instrum. Meth. A **419**, 726 (1998).
[24] J. Julin and T. Sajavaara, Nucl. Instrum. Meth. B **366**, 179 (2016).
[25] V. T. Jordanov and G. F. Knoll, Nucl. Instrum. Meth. B **345**, 337 (1994).
[26] A. N. James, K. A. Connell, and R. A. Cunningham, Nucl. Instrum. Meth. B **53**, 349 (1991).

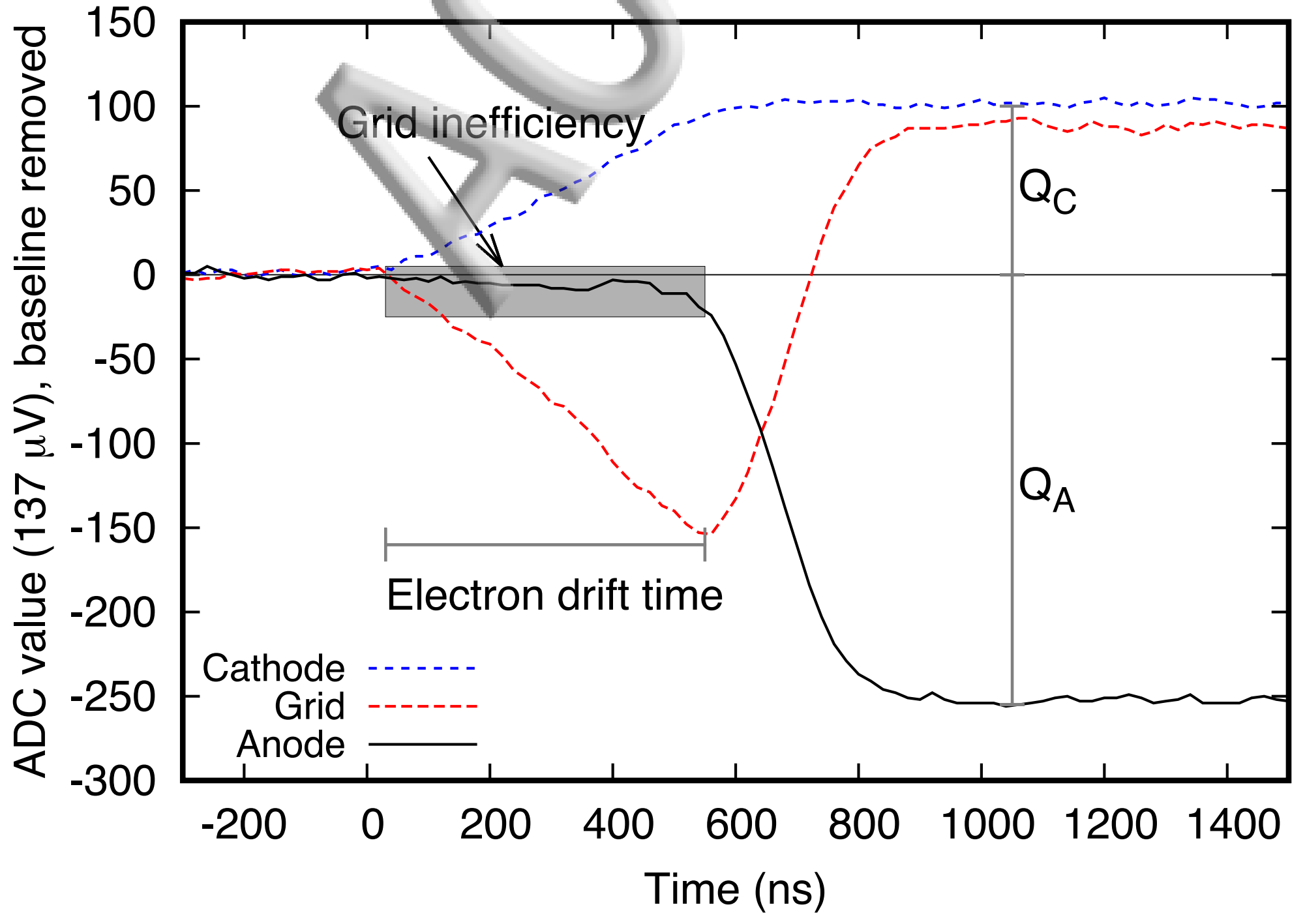
Grid inefficiency
Q_C
Q_A
Electron drift time
Cathode
Grid
Anode
ADC value (137 μV), baseline removed
Time (ns)
150
100
50
0
-50
-100
-150
-200
-250
-300
-200
0
200
400
600
800
1000
1200
1400

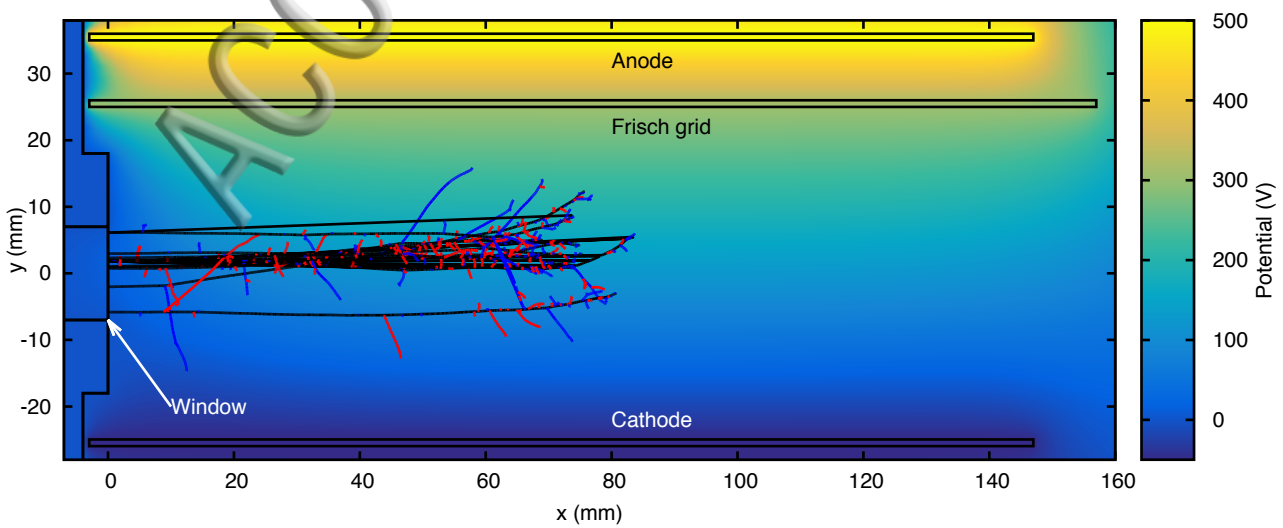
Anode
Frisch grid
Window
Cathode
y (mm)
x (mm)
Potential (V)
30
20
10
0
-10
-20
0
20
40
60
80
100
120
140
160
500
400
300
200
100
0

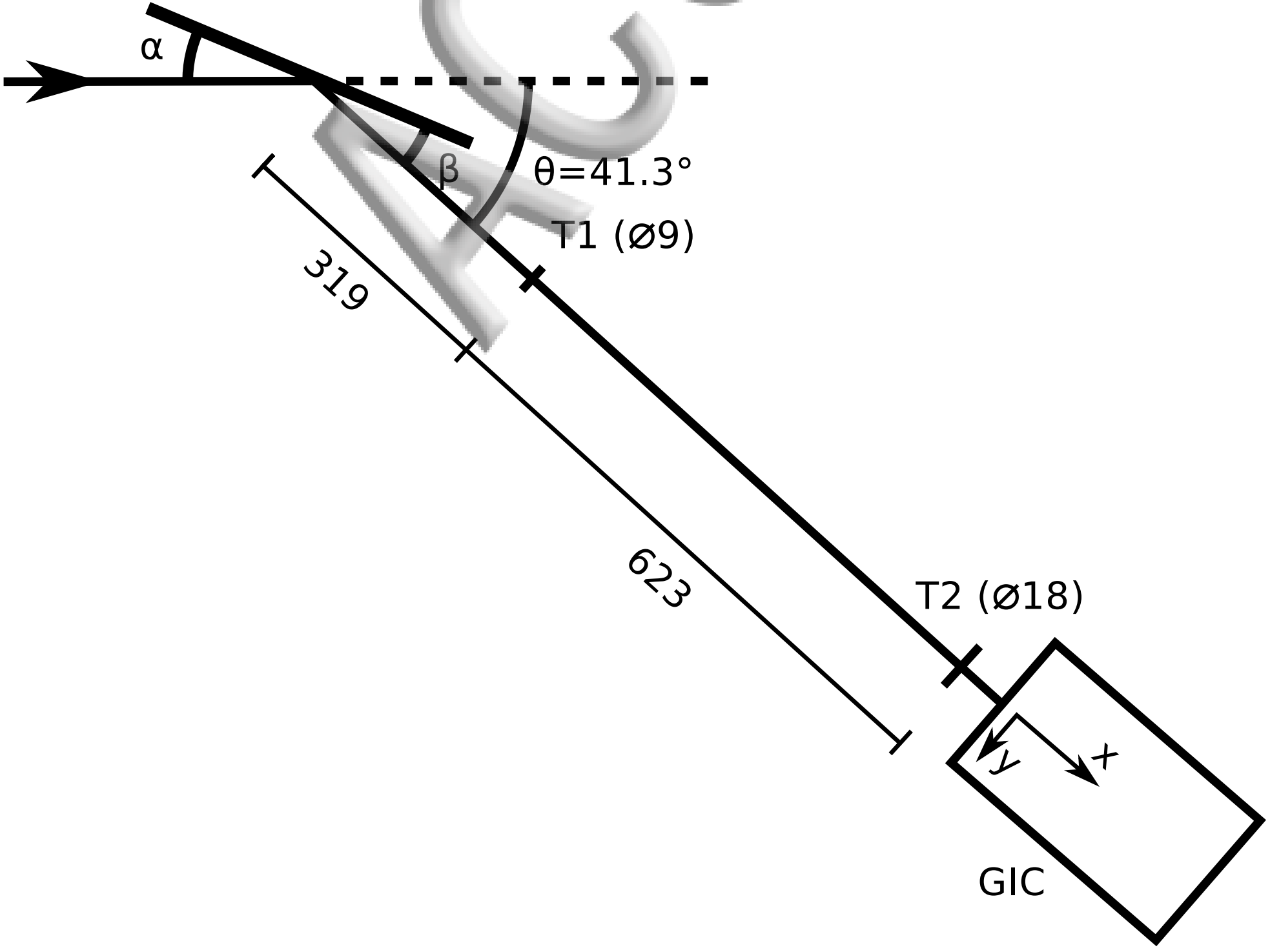
α
β
θ=41.3°
T1 (Ø9)
319
623
T2 (Ø18)
y
x
GIC

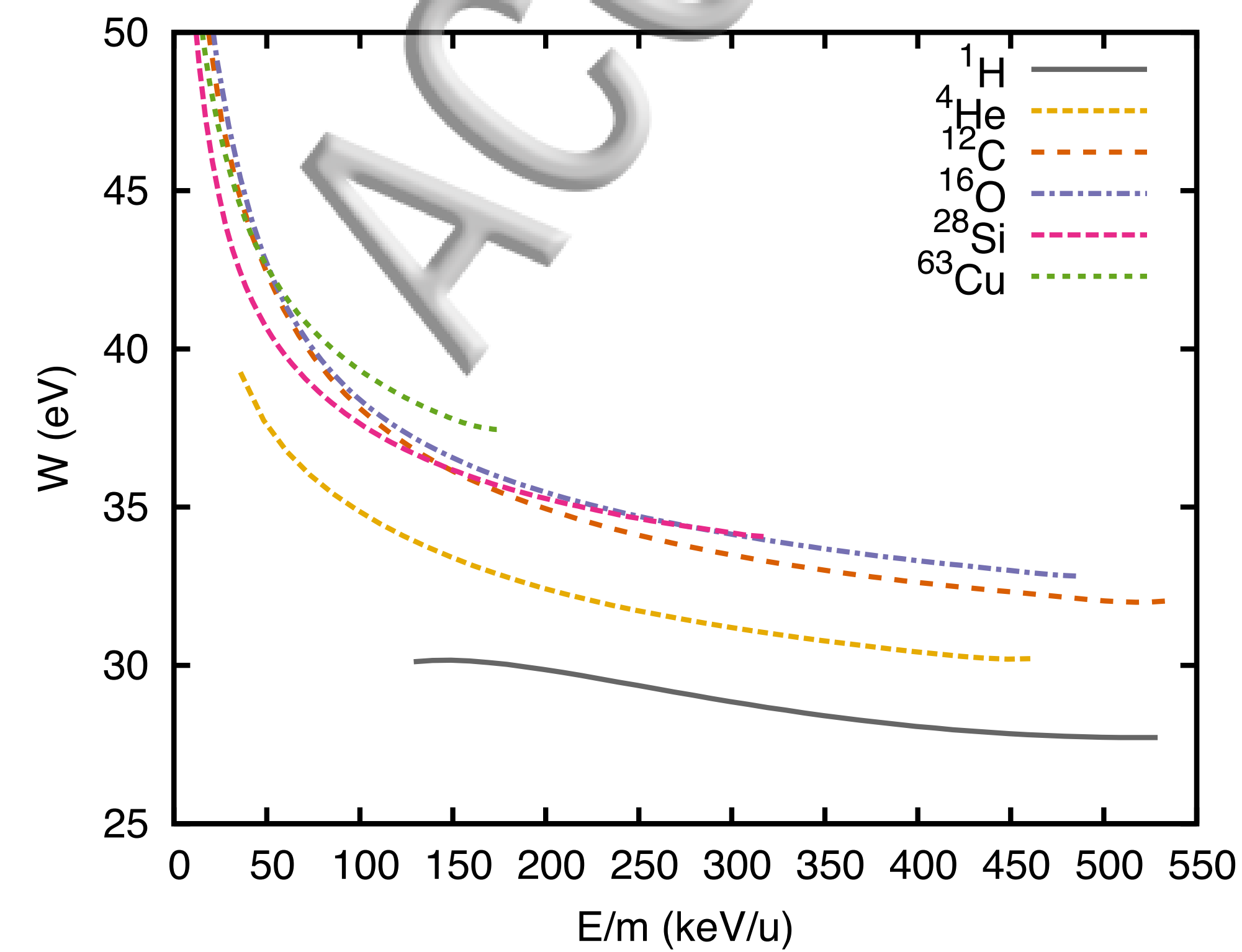
50
45
40
35
30
25
W (eV)
0
50
100
150
200
250
300
350
400
450
500
550
E/m (keV/u)
^{1}H
^{4}He
^{12}C
^{16}O
^{28}Si
^{63}Cu

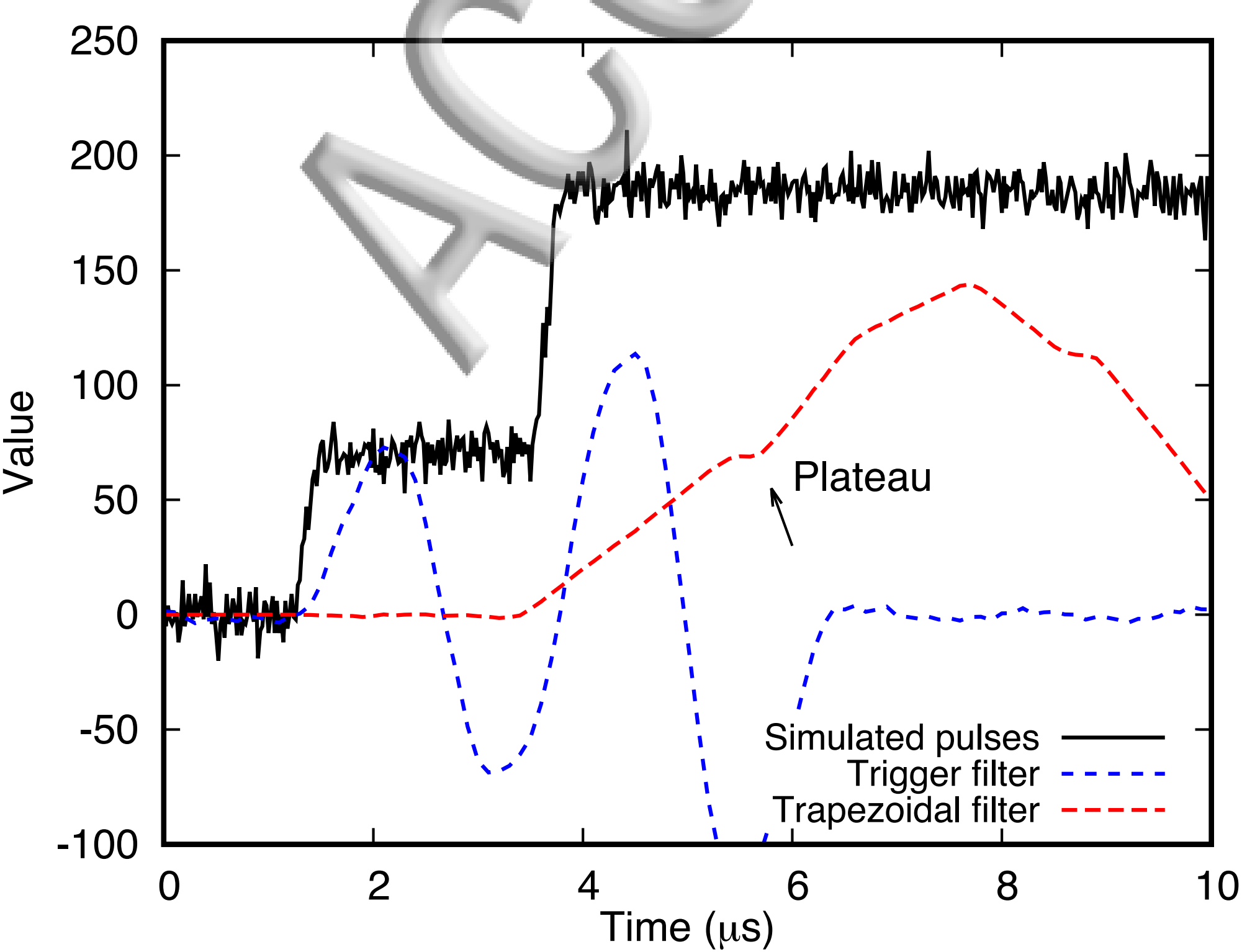
250
200
150
100
50
0
-50
-100
Value
0
2
4
6
8
10
Time (μs)
Plateau
Simulated pulses
Trigger filter
Trapezoidal filter

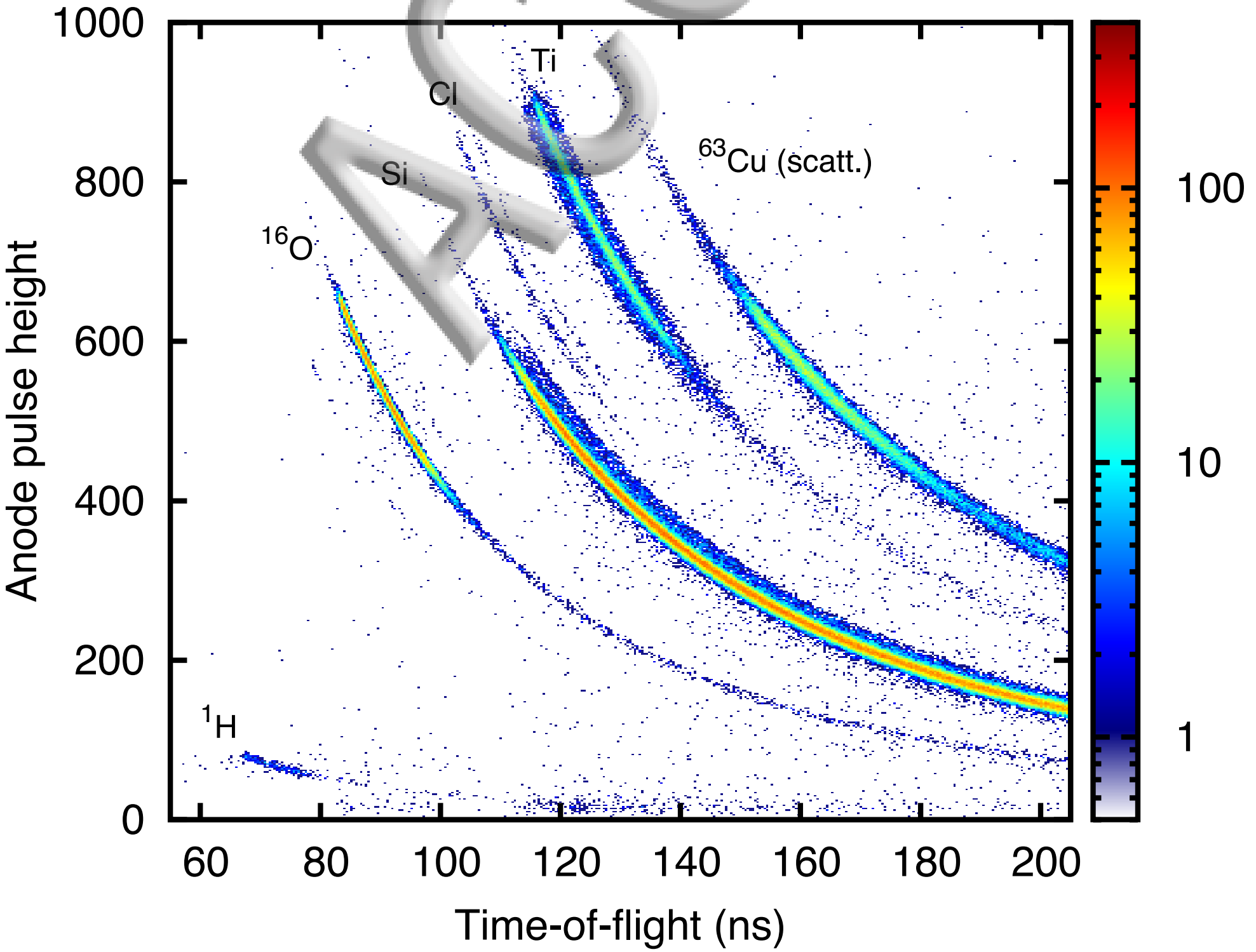
Ti
Cl
Si
^{16}O
^{63}Cu (scatt.)
^{1}H
Anode pulse height
Time-of-flight (ns)
0
200
400
600
800
1000
60
80
100
120
140
160
180
200
1
10
100

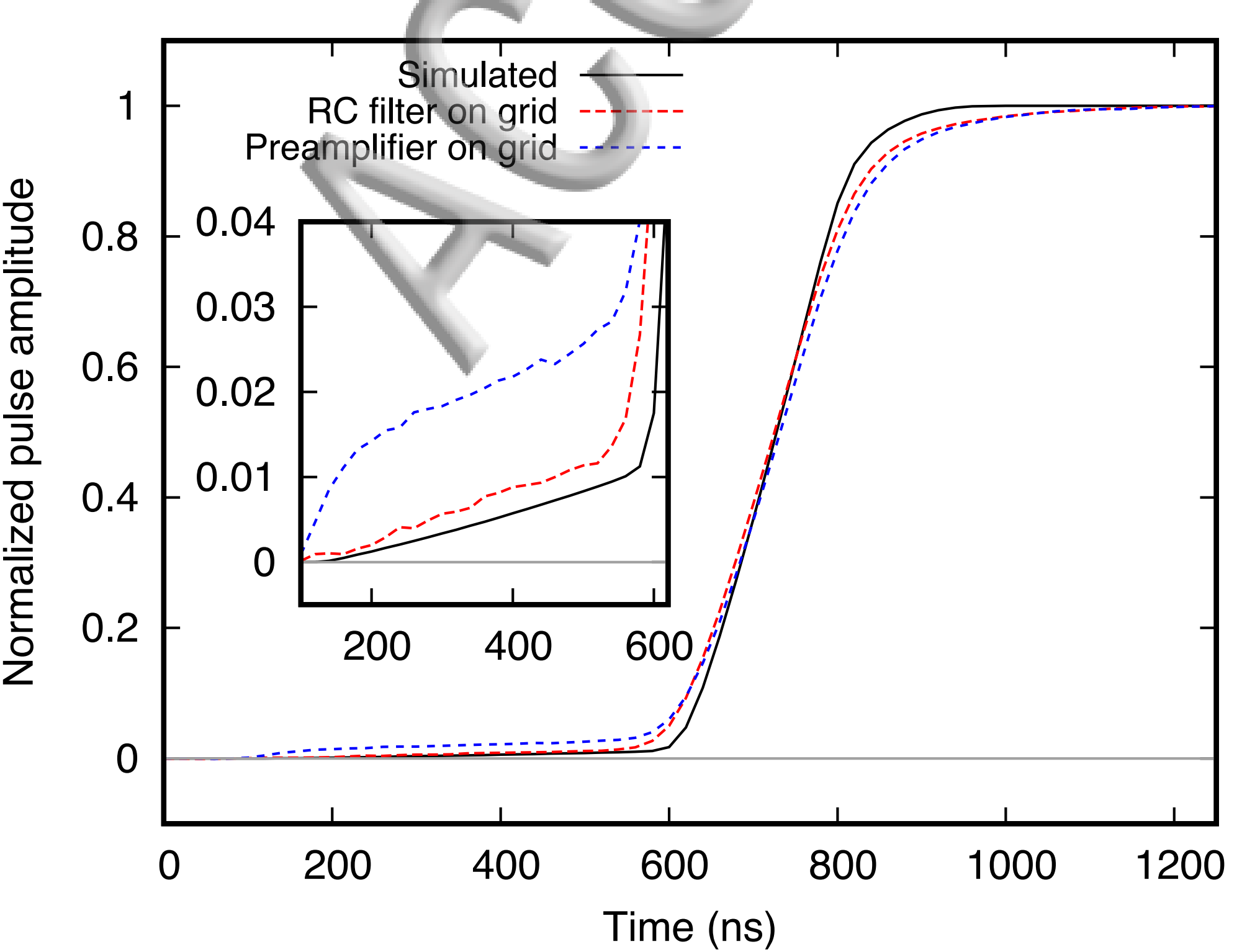
Simulated
RC filter on grid
Preamplifier on grid
Normalized pulse amplitude
Time (ns)
0
0.2
0.4
0.6
0.8
1
0
200
400
600
800
1000
1200
0.04
0.03
0.02
0.01
0
200
400
600

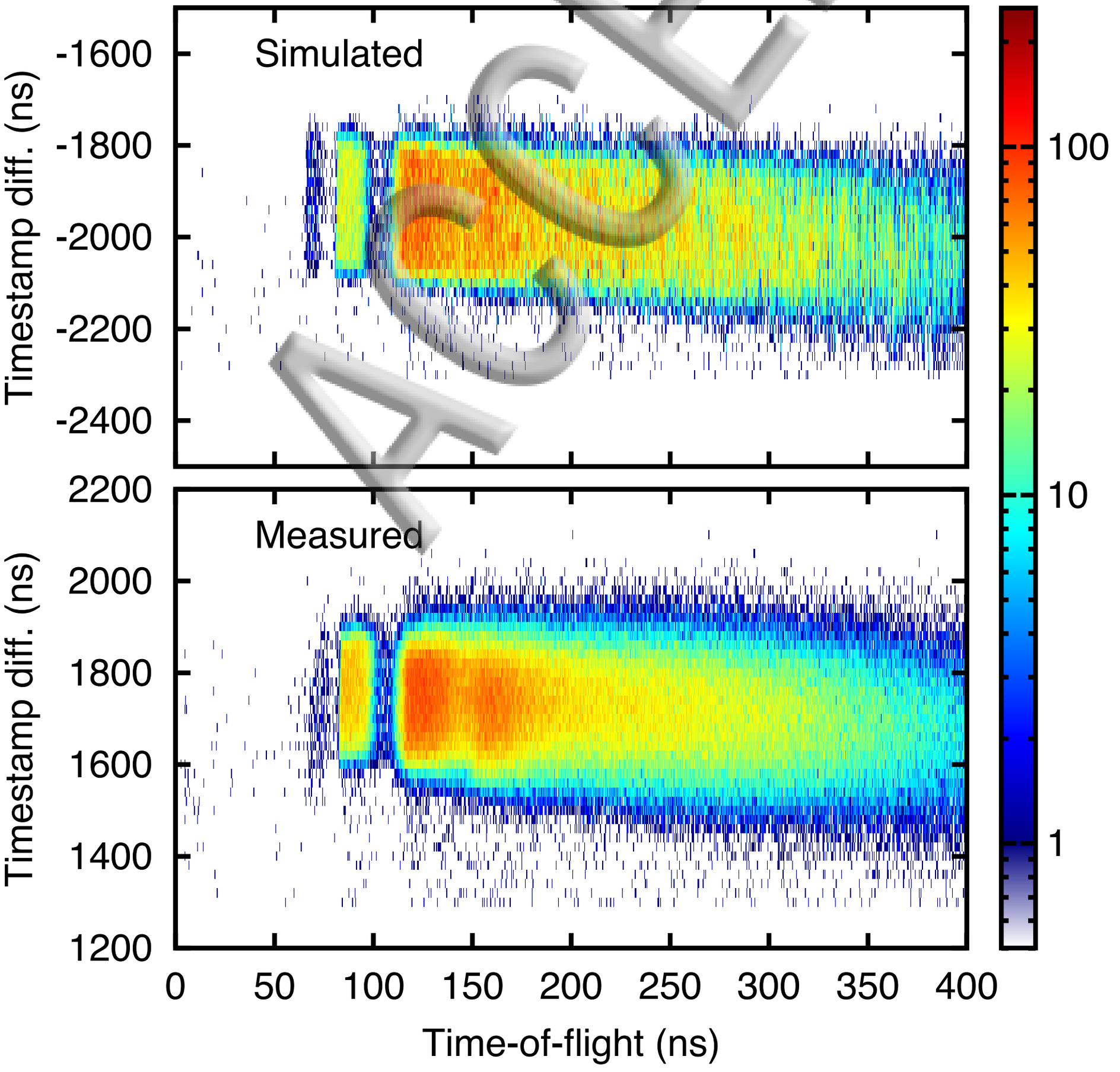
Simulated
Measured
-1600
-1800
-2000
-2200
-2400
2200
2000
1800
1600
1400
1200
Timestamp diff. (ns)
Timestamp diff. (ns)
0
50
100
150
200
250
300
350
400
Time-of-flight (ns)
100
10
1

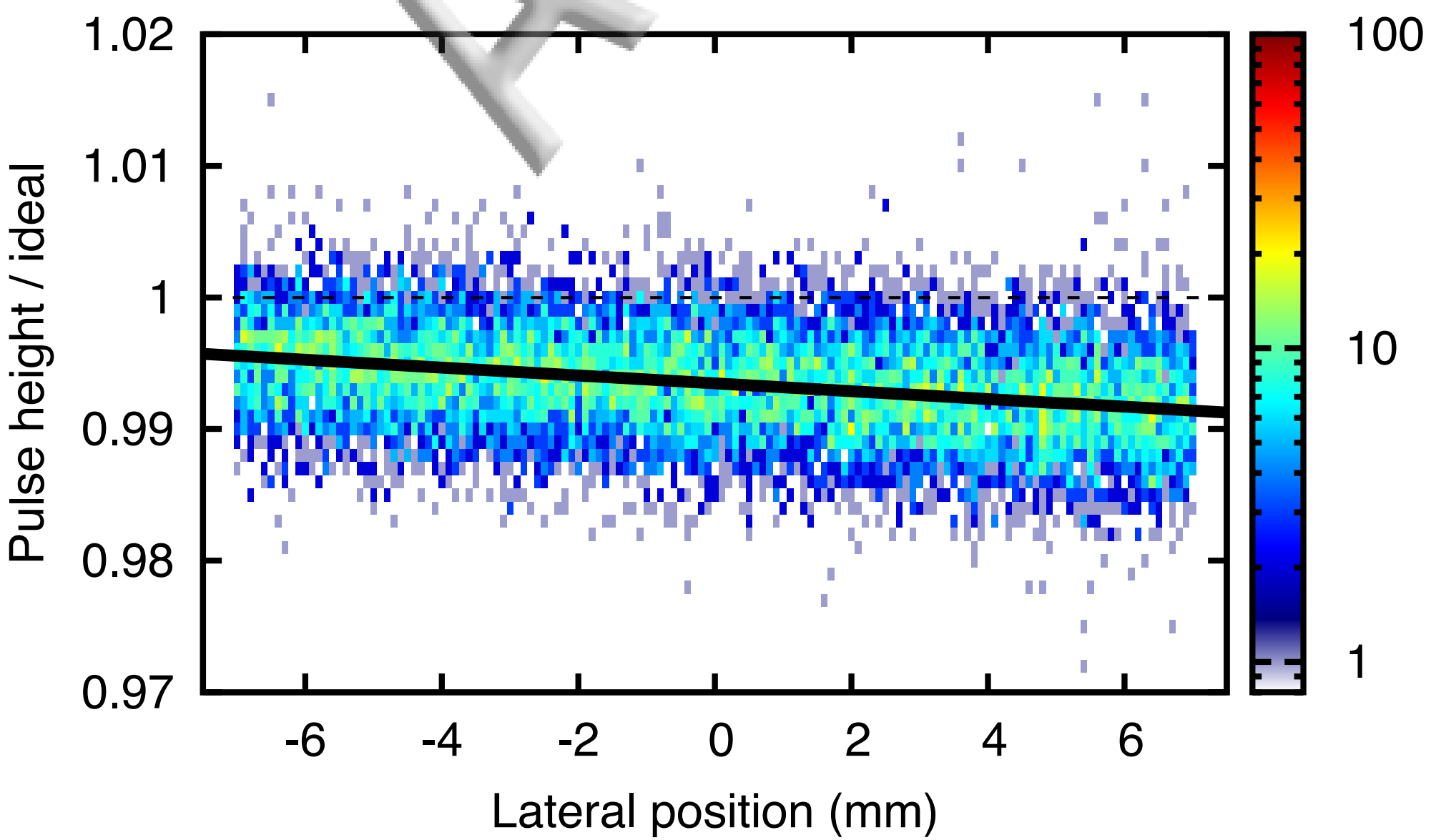
1.02
1.01
1
0.99
0.98
0.97
Pulse height / ideal
-6
-4
-2
0
2
4
6
Lateral position (mm)
100
10
1

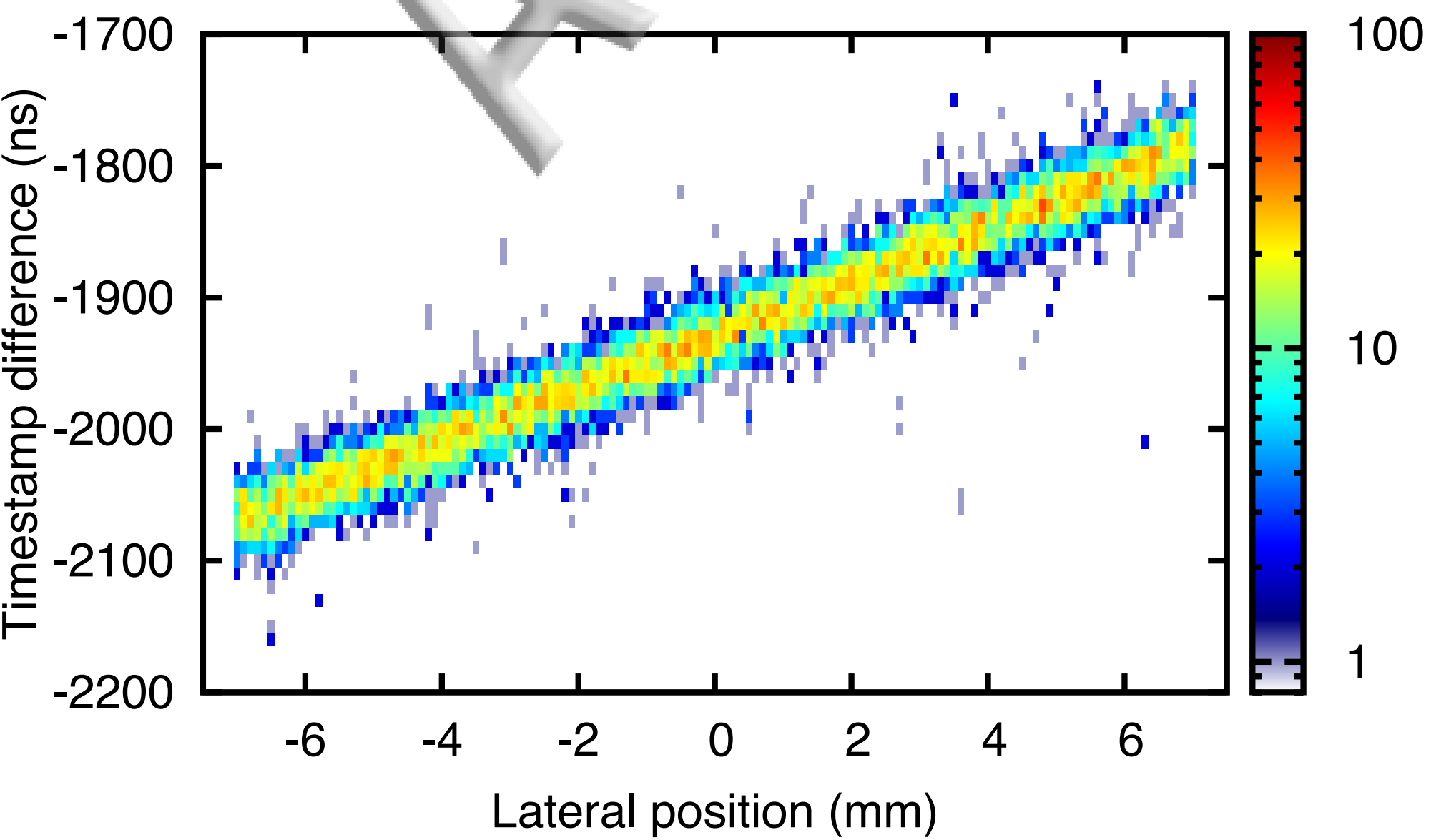
-1700
-1800
-1900
-2000
-2100
-2200
Timestamp difference (ns)
-6
-4
-2
0
2
4
6
Lateral position (mm)
100
10
1

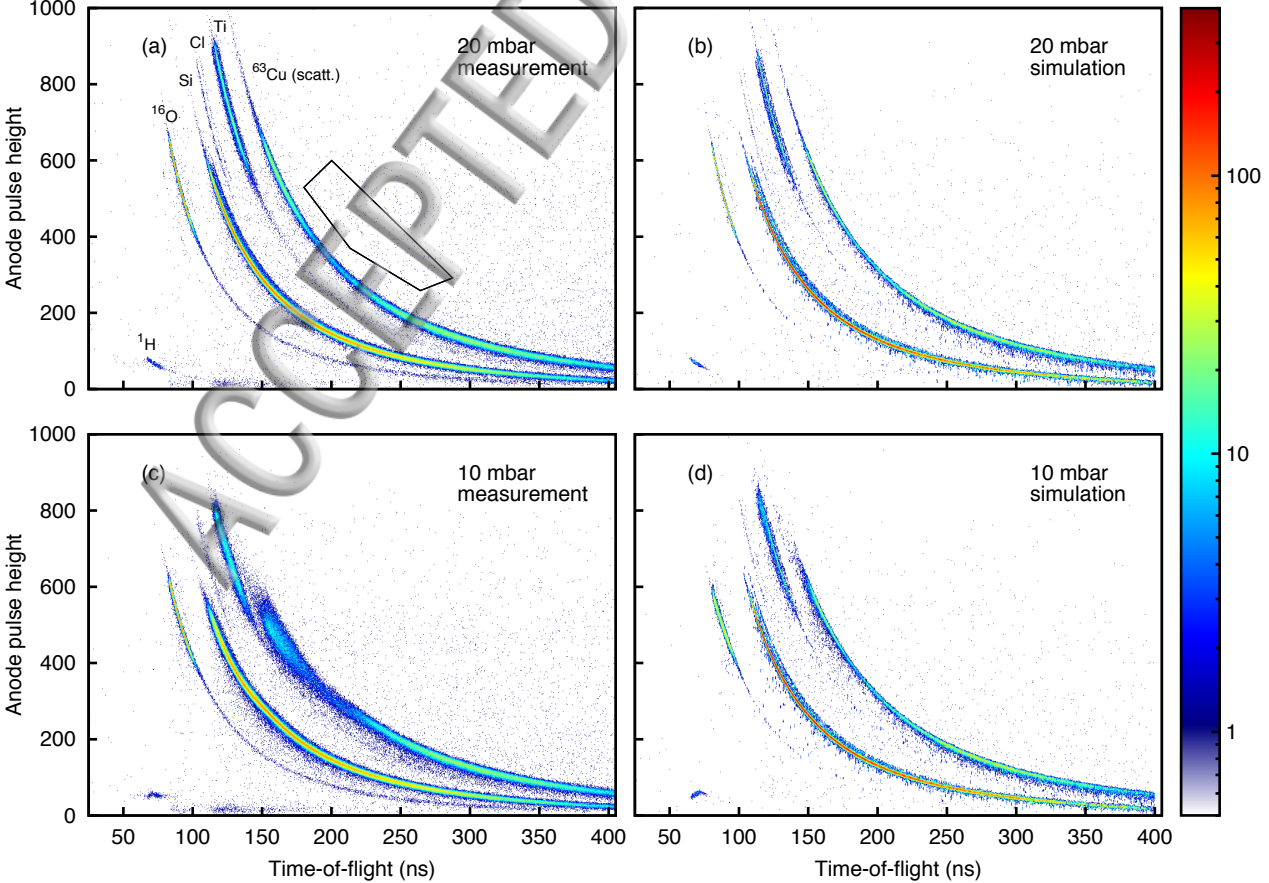
(a)
20 mbar
measurement
Ti
Cl
Si
^{63}Cu (scatt.)
^{16}O
^{1}H
(b)
20 mbar
simulation
(c)
10 mbar
measurement
(d)
10 mbar
simulation
Anode pulse height
Time-of-flight (ns)
0
200
400
600
800
1000
50
100
150
200
250
300
350
400
1
10
100

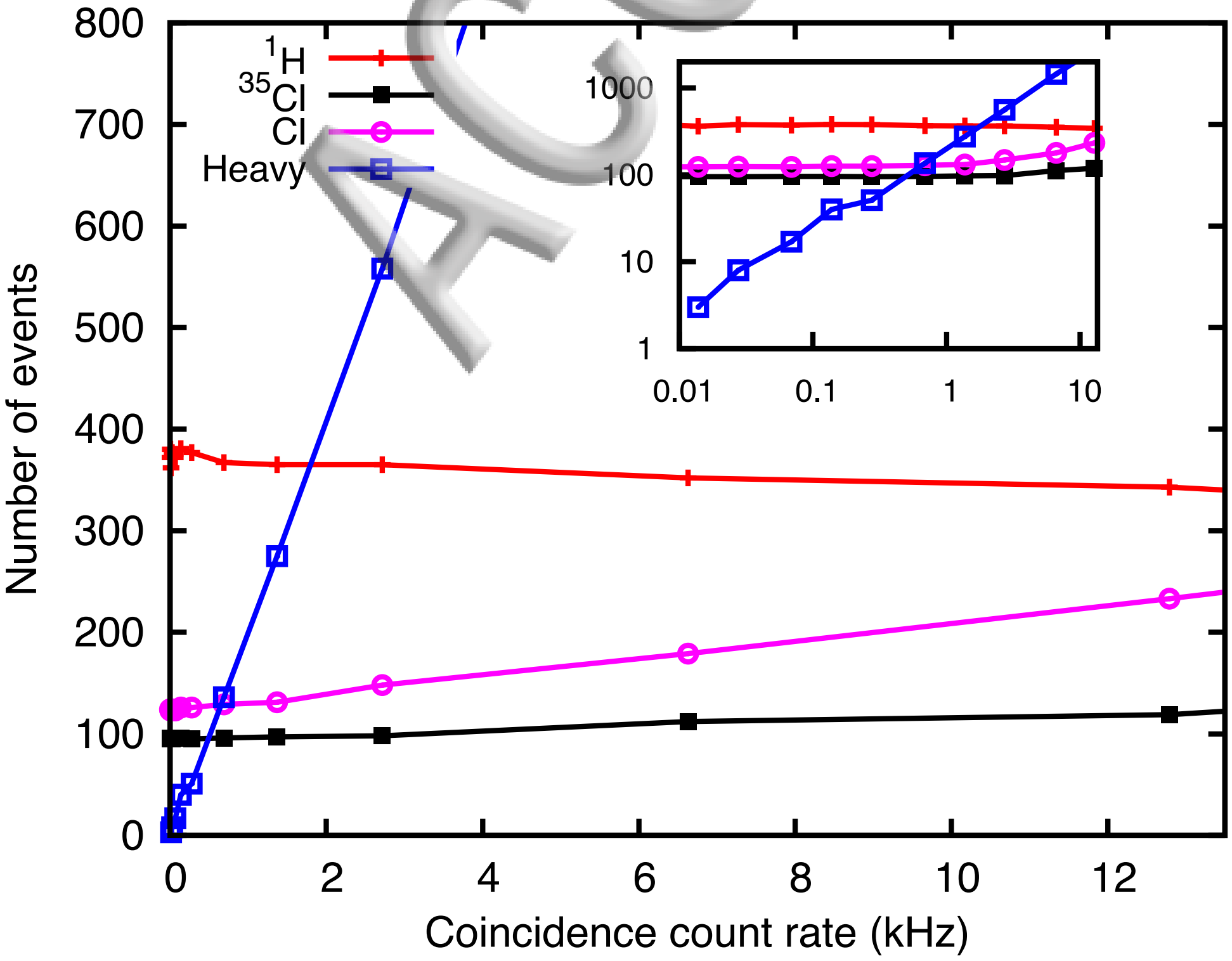
800
700
600
500
400
300
200
100
0
Number of events
0
2
4
6
8
10
12
Coincidence count rate (kHz)
^{1}H
^{35}Cl
Cl
Heavy
1000
100
10
1
0.01
0.1
1
10